CONDENSED
MATTER
PHYSICS

Effect of variable relative permittivity on the thermodynamics of asymmetric valency aqueous salts

A. O. Quiñones (iD) [1], Z. Abbas (iD) [2], C. W. Outhwaite (iD) [3], L. B. Bhuiyan (iD) [1]

[1] Laboratory of Theoretical Physics, Department of Physics, University of Puerto Rico, 17 Avenida Universidad, STE 1701, San Juan, Puerto Rico 00925-2537, USA

[2] Department of Chemistry and Molecular Biology, University of Gothenburg, Keningården 4, SE-41296, Gothenburg, Sweden

[3] School of Mathematical and Physical Sciences, University of Sheffield, Sheffield S3 7RH, UK

Experimentally determined empirical formulae for the concentration dependent relative permittivity of aqueous solutions of $MgCl_2$ and $NiCl_2$ are utilized to calculate the osmotic coefficient and the mean activity coefficient of these salts for a range of concentrations. The systems are modelled using the primitive model of electrolytes and analyzed using the symmetric Poisson-Boltzmann theory, the modified Poisson-Boltzmann theory, the mean spherical approximation, and the Monte Carlo simulations. Generally, the mean spherical approximation and the modified Poisson-Boltzmann theory reproduce the *benchmark* simulation data well up to ~1.6 mol/dm^3 or more in many instances, while the symmetric Poisson-Boltzmann results show discrepancies starting from ~0.25 mol/dm^3. Both the simulations and the theories tend to deviate from the corresponding experimental results beyond ~1 mol/kg.

Key words: *primitive model electrolytes, osmotic and mean activity coefficients, Monte Carlo simulations, symmetric and modified Poisson-Boltzmann theories*

1. Introduction

Osmotic and activity coefficients are two of the more important quantities in the thermodynamic description of charged fluids. From a practical point of view such data are relevant for many biological systems and for chemical industrial processes involving fluids [1–4]. Over the last seven decades or so a lot of experimental effort has been expended in chronicling such measurements (see for example, [5, 6] and references therein).

On the theoretical and numerical simulation front, the availability of powerful computational technology has been a boon to research in this field. The development of formal statistical mechanical theories of electrolytes in general has been greatly aided by numerical computer simulations of physical models, such data often being likened to as the *benchmark*. We quote here some of the more pertinent literature in this regard [7–13].

A widely used model of electrolytes and molten salts is a primitive model (PM). The ions are modelled as rigid spheres of arbitrary radii with an embedded charge of arbitrary valency at the centre of each ion. When the ionic sizes are the same, it is a restricted primitive model (RPM). It is noteworthy that the underlying model of the classical Debye-Hückel (DH) theory [14] is the RPM with vanishing radii. The conceptual simplicity and the ease of implementation of the DH makes it a popular first approximation in analyzing experimental data. The DH is a mean field theory and simulations supported by formal theories have shown over the years that its two basic deficiencies are the neglect of (i) fluctuation potential (inter-ionic correlations), and (ii) ionic exclusion volume effects. This makes the theory relevant only for
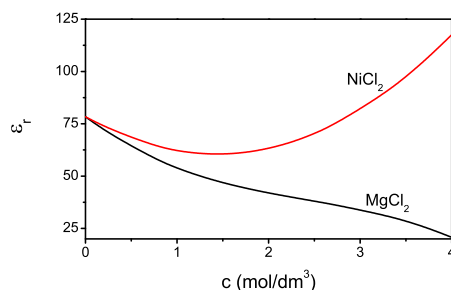
Figure 1. (Colour online) Variation of the relative permittivity ε_r as a function of concentration c [in (mol/dm^3)] for MgCl$_2$ and NiCl$_2$

monovalent systems at rather low concentrations. The PM (and the RPM), on the other hand, have proved useful in describing structure and thermodynamics of electrolytes at solution concentrations [7, 9, 15–20].

Traditionally, in the simulations and in the formal treatments of electrolytes, the relative permittivity ε_r (dielectric constant) is held fixed. Experiments, however, have revealed that the ε_r is not constant but is influenced by both the concentration and the temperature [5, 6]. Some limited theoretical works on variable ε_r were attempted using the DH theory [21, 22] and the MSA [23–26]. More recently, Abbas and Ahlberg [27] have done MC simulations for hydrogen halide and some alkali halides to calculate the osmotic coefficient ϕ and the mean ionic activity coefficients $y_\pm$ using concentration dependent and temperature dependent ε_r. In a previous paper [28], we applied the symmetric Poisson-Boltzmann (SPB), the modified Poisson-Boltzmann (MPB), and the MSA theories at the parameters of Abbas and Ahlberg's [27] simulations with encouraging results. The MSA, the MPB, and to a lesser extent the SPB could reproduce the MC data for ϕ and $y_\pm$ to a high degree of accuracy.

At a fundamental level, the simulations and the theories are based on the McMillan-Mayer (MM) formalism. The solvent is likened to a structureless continuum so that the ionic pair-potential is essentially an effective inter-ionic potential that incorporates solvent effects. The solution permittivity at infinite solute dilution is the permittivity of the pure solvent. It thus stands to reason, as Friedman [29] showed, that the effective potential should be concentration and temperature dependent. Friedman's analysis further demonstrated how non-pairwise terms in the effective potential lead to a concentration dependent ε_r. For a more detailed discussion of this point we refer the reader to [28]. Although analytical efforts to obtain a closed expression for ε_r have proved difficult [30–33], progress can be made by making recourse to experimental data. Indeed, this was done in the MC simulations of Abbas and Ahlberg [27] and in [28]. For each electrolyte treated, an empirical formula was used for ε_r based on the measured value of ε_r over a range of concentrations [6]. Such a scheme is also fairly straightforward to implement in both simulations and in the SPB, MPB, and MSA theories.

The electrolytes studied in [28] were all 1:1 symmetric valency systems. In the present work we extend the procedure to higher valency asymmetric 2:1 cases — MgCl$_2$ and NiCl$_2$. The empirical formulae for ε_r as function of concentration c, that we use for these salts, are as follows:

$$\varepsilon_r = 78.36 - 34c + 10.9c^2 - 1.5c^3 \qquad (1.1)$$

MgCl$_2$ [6], and

$$\varepsilon_r = 78.36 - 25c + 8.7c^2 \qquad (1.2)$$

for NiCl$_2$ [34].

There is another important difference between [28] and the present work. For instance, in [28], the ε_r for each of the electrolytes decreased with increasing concentration — the phenomenon known as *dielectric decrement* in the literature. By contrast, as can be seen in figure 1, although the ε_r decreases with c for MgCl$_2$, the ε_r for NiCl$_2$ initially decreases, reaches a minimum before increasing at higher concentrations. Apart from comparing the SPB, MPB, and MSA results with that of the MC simulations, we also compare both simulations and the theories with available experimental ϕ and $y_\pm$ data for MgCl$_2$ and NiCl$_2$ [35–38].

2. Model and Methods

2.1. Model

The PM used here is a two component system appropriate for a single electrolyte. The ions are mimicked by charged hard spheres of relevant sizes and charges in a dielectric medium of concentration dependent ε_r. The interionic pair potential is given by

$$u_{ij}(r) = \begin{cases} \infty & r < a_{ij} \\ e^2 Z_i Z_j / (4\pi\varepsilon_0\varepsilon_r r) & r > a_{ij}, \end{cases} \tag{2.1}$$

where $a_{ij} = a_i + a_j$, Z_s, a_s are the valency and radius of ionic species s respectively, e is the proton charge, and ϵ_0 is the vacuum permittivity.

2.2. Methods

The physical model outlined above was treated by MC simulations, and by the SPB, the MPB, and the MSA theories. Experimental results for the osmotic and activity coefficients are usually expressed in the molal scale rather than in the molar scale used in simulations and theories. We convert our (molar scale) data to molal scale using standard conversion relations. To be consistent with the conventional nomenclature in the literature, we use the symbols c and m to denote solution concentration in mol/dm^3 (molar scale) and mol/kg (molal scale), respectively, and the symbols y and γ to denote the activity coefficient in molar scale and in molal scale, respectively. To distinguish the osmotic coefficient in the two scales, we simply use ϕ_c and ϕ_m.

Conversion of "molarity" to "molality" and vice versa can be achieved using the relation [5]

$$m = \frac{c}{d - 10^{-3}cM}, \tag{2.2}$$

where M is the molar mass of the solute and d is the density of the solution.

Similarly, conversion of mean activity in molar scale to mean activity in molal scale and vice versa is accomplished by the relation [5]

$$\gamma_\pm = \frac{c}{m}\frac{y_\pm}{d_0}, \tag{2.3}$$

with d_0 being the density of the pure solvent. An analogous equation exists for the conversion of ϕ_c to ϕ_m.

2.2.1. MC simulations

The MC simulations were performed in a canonical (NVT) ensemble using a cubic box subject to periodic boundary conditions. The target concentration of the electrolyte solution was attained by trial-and-error varying the length of the edge of the box, while keeping the number of particles fixed. The osmotic coefficients were obtained from the calculated pair correlation (radial distribution) functions and the virial expression [7], while the activity coefficients were evaluated through a modified Widom particle insertion technique [15, 39]. Specifically, the Widom method [15] states that a non-perturbing particle of species s inserted at a random position r will have the individual activity coefficient y_s given by

$$\ln y_s = -\ln\langle\{\exp[-\beta\Delta U_s(r)]\}\rangle. \tag{2.4}$$

Here, $\beta = 1/(k_\mathrm{B}T)$, with k_B being the Boltzmann's constant and T being the absolute temperature. The exponential term enclosed in brackets is the ensemble average of the energy change, ΔU_s due to the particle addition. This method provides a direct calculation of the chemical potential. However, the original Widom method becomes less accurate when dealing with ionic systems of finite sizes, since the addition of a charged particle will violate electroneutrality in the MC cell. This effect can be considerably reduced by using a charge rescaling method. Charge rescaling is a simple method to re-establish electroneutrality in the computation cell. This method has shown good results for symmetric
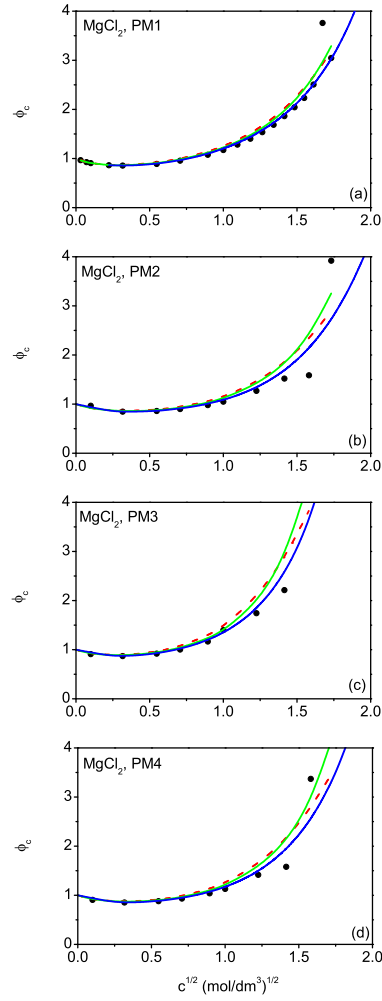
Figure 2. (Colour online) MPB, SPB, MSA, and MC osmotic coefficient ϕ_c (in molar scale) as function of square root of concentration $c^{1/2}$ (in (mol/dm^3)$^{1/2}$) for MgCl$_2$ using the PM with a concentration dependent dielectric constant ε_r. In all of the sub-figures, dashed red line SPB, solid green line MPB, solid blue line MSA, black filled circles MC; **(a)** PM1, $a_{\text{Mg}^{2+}} = 2.95 \cdot 10^{-10}$ m, $a_{\text{Cl}^-} = 1.81 \cdot 10^{-10}$ m, fixed ε_r, **(b)** PM2, $a_{\text{Mg}^{2+}} = 2.95 \cdot 10^{-10}$ m, $a_{\text{Cl}^-} = 1.81 \cdot 10^{-10}$ m, variable ε_r, **(c)** PM3, $a_{\text{Mg}^{2+}} = 3.50 \cdot 10^{-10}$ m, $a_{\text{Cl}^-} = 1.81 \cdot 10^{-10}$ m, variable ε_r, **(d)** PM4, $a_{\text{Mg}^{2+}} = 3.15 \cdot 10^{-10}$ m, $a_{\text{Cl}^-} = 1.81 \cdot 10^{-10}$ m, variable ε_r.

as well as for asymmetric electrolytes. The mean activity coefficient $y_\pm$ is now obtained from the y_s, following the standard practice [10].

The contact value of the pair correlation function $g_{st}(a_{st})$ between two ions s and t needed in the calculation of the ϕ_c is obtained by a second order polynomial fit to $g_{st}(r)$ for r close to contact. Further details of the MC method can be found in reference [15] and in some relevant literature cited there.

Explicitly, the expression used for ϕ_c is taken from reference [40] [see equation (4.4)], which can be written, using our notations (see also references [41–43]), as

$$\phi_c = 1 + \frac{2\pi}{3\rho} \sum_s \sum_t \rho_s \rho_t g_{st}(a_{st}) a_{st}^3 + \frac{\beta E}{3\rho}, \qquad (2.5)$$

where E is the (MC) excess energy, ρ_s is the mean number density of ions of type s, and $\rho = \sum_s \rho_s$ with the summation being over the number of ionic species. In the simulation calculations for ϕ_c, the
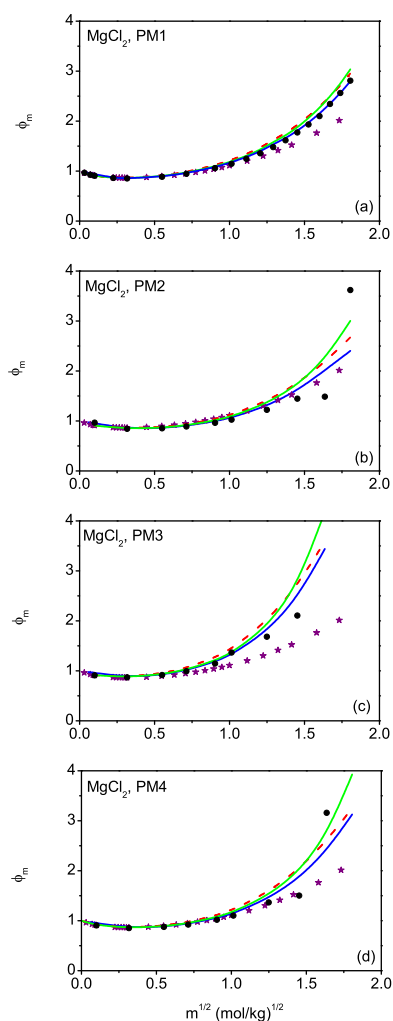
Figure 3. (Colour online) MPB, SPB, MSA, and MC osmotic coefficient ϕ_m (in molal scale) as function of square root of concentration $m^{1/2}$ (in $(\text{mol/kg})^{1/2}$) for $MgCl_2$ using the PM with a concentration dependent dielectric constant ε_r. In all of the sub-figures, dashed red line SPB, solid green line MPB, solid blue line MSA, black filled circles MC, purple stars experiment [6]. Rest of the legend as in figure 2.

excess energy term E was evaluated via its representation in terms of the $g_{st}(r)$ rather than the mean electrostatic potential [7].

As a check on the numerics we repeated the calculations in the grand canonical ensemble. The results for the thermodynamic data from the two ensembles were within statistical error of each other. We used a large number of particles of the order $\sim 10^3$ and generated a large number of MC configurations of the order $\sim 10^8$. The first 10% were used for system equilibration, while the rest were used in taking statistics. Concentration dependence of the ε_r was ensured by using experimentally measured values of the quantity at different concentrations for the salt solutions treated.

2.2.2. SPB and MPB theories

The SPB and MPB constitute potential formulations of the theory to describe electrolyte solutions. An important difference between the classical, non-linear Poisson-Boltzmann (PB) theory and the SPB, MPB is that while in the former the pair correlation function $g_{ij}(r)$ between two ions i and j is asymmetric, for instance, $g_{ij}(r) \neq g_{ji}(r)$, with respect to an interchange of indices, for any asymmetry in the system,

the latter two are devoid of this defect. The SPB is still a mean-field theory, although, as we will see later, some hard core effects are taken into account through the exclusion volume envelope. The MPB accounts for both the ionic exclusion volume effects and for the fluctuation potential missing in the SPB. The development of SPB and MPB formalisms over the years have been detailed in the literature (see for example [41–44]). We will therefore be brief and simply outline the principal equations involved in the theories.

The starting point is the Poisson's equation

$$\nabla^2 \psi_s(1;2) = -\frac{|e|}{\varepsilon_0 \varepsilon_r} \sum_t Z_t \rho_t g_{st}(r_{st}). \tag{2.6}$$

Here, $\psi_s(1;2)$ is the mean electrostatic potential about an ion s at $\mathbf{r}_1$ at a field point $\mathbf{r}_2$, g_{st} is the pair correlation function for the ion pair s and t with separation $r_{st} = |\mathbf{r}_1 - \mathbf{r}_2|$. Note that we will be dealing here with single electrolytes so that $s = i, j$ (i, j being $+, -$ or $-, +$).

For the PM, in the SPB theory, the symmetrized $g_{st}(r)$ ($r = r_{st}$) is developed as

$$g_{st}(r) = g_{st}^0(r) \exp\left\{-\frac{\beta e}{2} \left[Z_s(\psi_t(r) + \psi_t^0(r)) + Z_t(\psi_s(r) + \psi_s^0(r))\right]\right\}, \tag{2.7}$$

where $\psi_s^0(r) = \psi_s(r; Z_s = 0)$ is the (discharged) potential at a distance r from the discharged ion s. The g_{st}^0 in the above equation is the exclusion volume term, which is the pair correlation between two discharged ions in a sea of fully charged ions.

In the MPB, the $g_{st}(r)$ is given by

$$g_{st}(r) = g_{st}^0(r) \exp\left\{-\frac{\beta e}{2} \left[Z_s(L_t(u_t) + L_t(u_t|Z_t = 0)) + Z_t(L_s(u_s) + L_s(u_s|Z_s = 0))\right]\right\}. \tag{2.8}$$

Here, $u_s = r\psi_s(r)$, and assuming without loss of generality that $a_i \leqslant a_j$, we have

$$L_s(u) = \frac{1}{2r(1 + \kappa a_{is})} \left[u(r + a_{is}) + u(r - a_{is}) + \kappa \int_{r-a_{is}}^{r+a_{is}} u(R) \mathrm{d}R\right], \tag{2.9}$$

with the ion i having the smallest radius. The Debye-Hückel parameter κ is given by

$$\kappa = \left[\frac{e^2 \beta}{\varepsilon_0 \varepsilon_r} \sum_s Z_s^2 \rho_s\right]^{1/2}. \tag{2.10}$$

The exclusion volume term g_{is}^0 was approximated by the Percus-Yevick uncharged pair distributions [8, 45, 46] and their corrections due to Verlet and Weis [47]. The equations (2.6) and (2.7) constitute the SPB equation, while the equations (2.6),(2.8)–(2.10) constitute the MPB equation.

To calculate the ϕ_c and $y_\pm$ in the SPB and MPB theories, we have used the virial route and the Guntelberg charging route, respectively [42, 43, 48]. These routes represent the optimum thermodynamic ones for these theories.

The expression for ϕ_c used in both the SPB and MPB is that given above, equation (2.5), where the excess energy E in terms of the mean electrostatic potential is

$$E = \frac{e}{2} \sum_s Z_s \rho_s \left[\psi_s(a_{is}) - \frac{eZ_s}{4\pi\varepsilon_0 \varepsilon_r a_{is}}\right]. \tag{2.11}$$

The individual ionic activity is written in terms of the hard sphere (HS) and electrical (el) parts.

$$\ln y_s = \ln y_s^{\mathrm{HS}} + \ln y_s^{\mathrm{el}}, \tag{2.12}$$

$$\ln y_s^{\mathrm{el}} = e\beta Z_s \int_0^1 \mathrm{d}\lambda \left[\psi_s(a_{is}, \lambda) - \frac{\lambda e Z_s}{4\pi\varepsilon_0 \varepsilon_r a_{is}}\right], \tag{2.13}$$
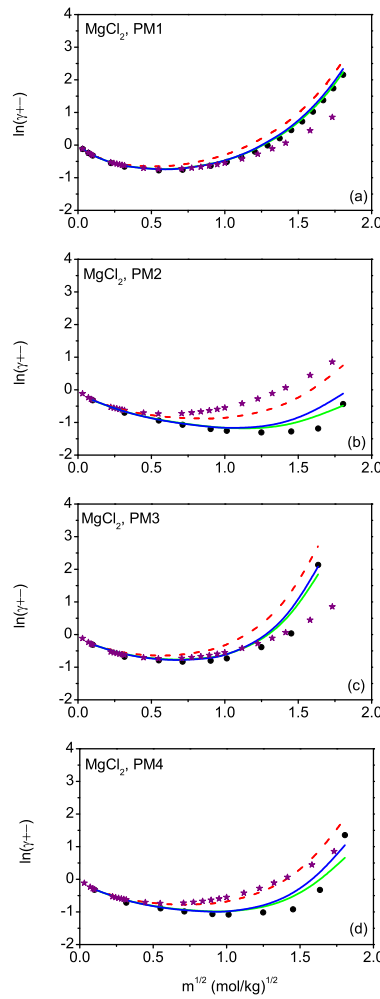
Figure 4. (Colour online) MPB, SPB, MSA, and MC mean activity coefficient $y_{\pm}$ (in molar scale) as function of square root of concentration $c^{1/2}$ (in $(mol/dm^3)^{1/2}$) for $MgCl_2$ using the PM with a concentration dependent dielectric constant ε_r. In all of the sub-figures, dashed red line SPB, solid green line MPB, solid blue line MSA, black filled circles MC. Rest of the legend as in figure 2.

with the hard sphere contribution being obtained from the Ebeling and Scherwinski results [49]. As before with MC, the mean activity $y_{\pm}$ is obtained from the y_s in the usual manner [10]. We note that since a_i is fixed as the smallest ion [see text below equation (2.9)], so in the right hand side of equation (2.11) whenever we have a_{is}, s is regarded as variable and a_{is} could be either a_{ii} or a_{ij}. E is simply the excess energy independent of s, while in equation (2.13) $\ln y_s^{\text{el}}$ is the individual activity (electrical part) for ions of type s. With equal ion sizes the expressions for E and $\ln y_s^{\text{el}}$ reduce to those in reference [50].

2.2.3. MSA

The MSA is a linear, integral equation theory with the advantage that it is analytically tractable [12, 51]. The thermodynamic quantities of interest such as the internal energy, the osmotic coefficient, and the activity coefficients have got closed analytic forms [52, 53].

The starting point here is the homogeneous Ornstein-Zernike (OZ) equation

$$h_{st}(r_{st}) = c_{st}(r_{st}) + \sum_m \int h_{sm}(r_{sm})c_{mt}(r_{mt})\mathrm{d}\mathbf{r}_3, \qquad (2.14)$$
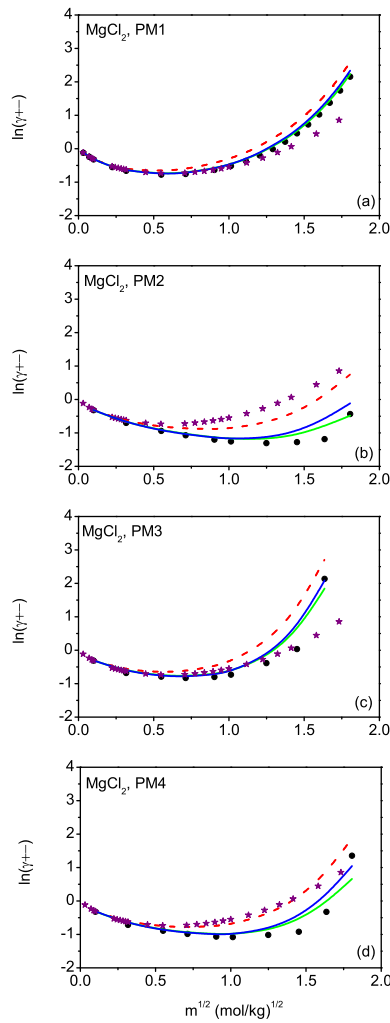
Figure 5. (Colour online) MPB, SPB, MSA, and MC mean activity coefficient $\gamma_\pm$ (in molal scale) as function of square root of concentration $m^{1/2}$ (in (mol/kg)$^{1/2}$) for MgCl$_2$ using the PM with a concentration dependent dielectric constant ε_r. In all of the sub-figures, dashed red line SPB, solid green line MPB, solid blue line MSA, black filled circles MC, purple stars experiment [6]. Rest of the legend as in figure 2.

where $r_{sm} = |\mathbf{r}_1 - \mathbf{r}_3|$, and $h_{st} (= g_{st} - 1)$ and c_{st} are the total and direct correlation functions, respectively.

The OZ equation together with the following (MSA) closure relations comprise the MSA theory,

$$g_{ij}(r) = 0, \quad r < a_{ij}, \tag{2.15}$$

$$c_{ij}(r) = -\beta u_{ij}(r), \quad r > a_{ij}. \tag{2.16}$$

Note that equation (2.15) is an exact condition, while equation (2.16) is an approximation. For the MSA, the energy route is the most accurate thermodynamic route and hence this was employed [52, 53] to evaluate the ϕ_c and $y_\pm$.

3. Results

The SPB and MPB equations were solved numerically using a previously used quasi-linearization iteration procedure [54]. This is a robust technique which has proved useful in earlier works (see for
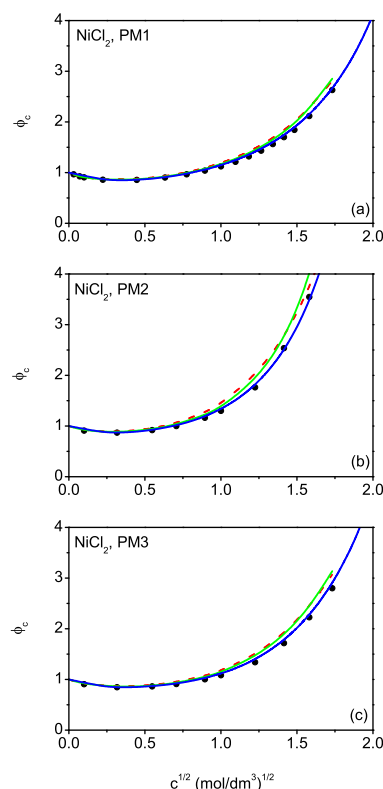
Figure 6. (Colour online) MPB, SPB, MSA, and MC osmotic coefficient ϕ_c (in molar scale) as function of square root of concentration $c^{1/2}$ (in $(\text{mol/dm}^3)^{1/2}$) for $NiCl_2$ using the PM with a concentration dependent dielectric constant ε_r. In all of the sub-figures, dashed red line SPB, solid green line MPB, solid blue line MSA, black filled circles MC; **(a)** PM1, $a_{Ni^{2+}} = 2.80 \cdot 10^{-10}$ m, $a_{Cl^-} = 1.81 \cdot 10^{-10}$ m, fixed ε_r, **(b)** PM2, $a_{Ni^{2+}} = 3.40 \cdot 10^{-10}$ m, $a_{Cl^-} = 1.81 \cdot 10^{-10}$ m, variable ε_r, **(c)** PM3, $a_{Ni^{2+}} = 2.90 \cdot 10^{-10}$ m, $a_{Cl^-} = 1.81 \cdot 10^{-10}$ m, variable ε_r.

example [41–43, 48, 55]). The MSA results for the osmotic and activity coefficients were obtained from their analytic expressions [12, 52, 53]. The necessary hard sphere contributions to the activity coefficients were obtained from the work of Ebeling and Scherwinski [49].

We present the results here for $\phi_c(\phi_m)$ and $y_\pm(\gamma_\pm)$ for $MgCl_2$ and $NiCl_2$ solutions with concentration dependent ε_r (cf. equations (1.1) and (1.2)) at $T = 298$ K. Some results at fixed $\varepsilon_r = 78.36$ have also been included for comparison purposes. For each of the salts, different combinations of cation and anion radii were used. In the MC simulations, the adopted strategy of keeping the anion size equal to its crystallographic value, while the cation size is optimized to fit the experimental data, was based on the dielectric relaxation spectroscopic work on electrolyte solutions by Buchner and Hefter [56]. They have shown, for example, that Cl^- ions have vanishingly small hydration shells around them, whereas, the Mg^{2+} ions display strong hydration. We have used four such sets for $MgCl_2$:

(i)   PM1 $a_{Mg^{2+}} = 2.95 \cdot 10^{-10}$ m, $a_{Cl^-} = 1.81 \cdot 10^{-10}$ m, fixed ε_r,

(ii) PM2 $a_{Mg^{2+}} = 2.95 \cdot 10^{-10}$ m, $a_{Cl^-} = 1.81 \cdot 10^{-10}$ m, variable ε_r,

(iii) PM3 $a_{Mg^{2+}} = 3.50 \cdot 10^{-10}$ m, $a_{Cl^-} = 1.81 \cdot 10^{-10}$ m, variable ε_r,

(iv) PM4 $a_{Mg^{2+}} = 3.15 \cdot 10^{-10}$ m, $a_{Cl^-} = 1.81 \cdot 10^{-10}$ m, variable ε_r

and three sets for $NiCl_2$:

(i)   PM1 $a_{Ni^{2+}} = 2.80 \cdot 10^{-10}$ m, $a_{Cl^-} = 1.81 \cdot 10^{-10}$ m, fixed ε_r,

(ii) PM2 $a_{Ni^{2+}} = 3.40 \cdot 10^{-10}$ m, $a_{Cl^-} = 1.81 \cdot 10^{-10}$ m, variable ε_r,

(iii) PM3 $a_{Ni^{2+}} = 2.90 \cdot 10^{-10}$ m, $a_{Cl^-} = 1.81 \cdot 10^{-10}$ m, variable ε_r.
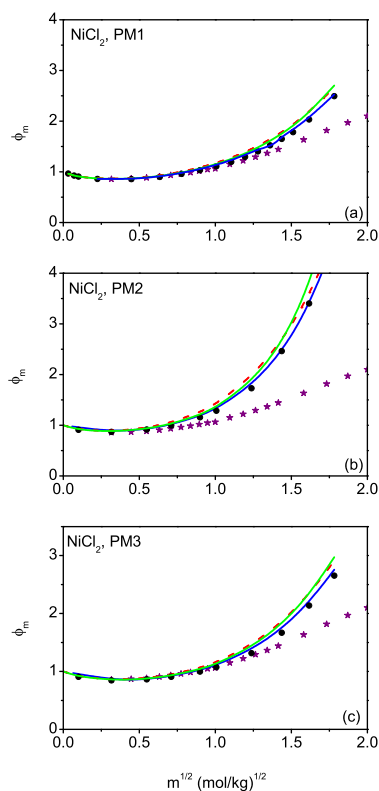
Figure 7. (Colour online) MPB, SPB, MSA, and MC mean activity coefficient $\gamma_{\pm}$ (in molal scale) as function of square root of concentration $m^{1/2}$ [in $(mol/kg)^{1/2}$] for $NiCl_2$ using the PM with a concentration dependent dielectric constant ε_r. In all of the sub-figures, dashed red line SPB, solid green line MPB, solid blue line MSA, black filled circles MC, purple stars experiment [6]. Rest of the legend as in figure 6.

These radii were also used in the SPB, MPB, and MSA applications. The best-fit to the experimental data [35–38] is achieved by PM4 for $MgCl_2$ and by PM3 for $NiCl_2$.

Figures 2 and 3 show the osmotic coefficient of $MgCl_2$ in molar scale (as a function of $c^{1/2}$) and in molal scale (as a function of $m^{1/2}$), respectively, for the four PM's. The theoretical curves are all consistent with each other across the four models. In general, the theories predict the simulation data well up to $c \sim 1.6$ mol/dm^3. The SPB curves tend to deviate more, as expected, at higher concentrations when the neglect of the fluctuation potential becomes more consequential. For the PM2–PM4, the MC data show a little noise beyond $c \sim 2.25$ mol/dm^3. Indeed, in PM4 at $c = 3$ mol/dm^3, the MC $\phi_c = 26.52$, which may well be an outlier. The corresponding curves in molal scale in figure 3 are compared with the experimental $MgCl_2$ ϕ_m data [6]. The simulations and the theoretical predictions appear relatively closer to the experimental data in PM1 and in PM2 than they do in PM3 and PM4. In the latter two cases the simulations begin to show deviations from the experiments beyond $m \sim 1$ mol/kg.

We now turn to figures 4 and 5, which illustrate the mean activity coefficient of $MgCl_2$, again in molar and molal scales, respectively. Apropos of what we saw in figure 2, the theories, with the exception of the SPB, reproduce the MC data closely for PM1. For PM2–PM4, notwithstanding some statistical noise in the simulation data at higher concentrations, the theoretical curves begin to deviate beyond $c \sim 1.6$ mol/dm^3. The deviation of SPB is more than that of MSA or MPB. The trends of these curves in figure 5 are similar, with the simulations and the theories being relatively closer to the experimental data in PM1 and PM3 up to ~ 1.6 mol/kg. It is of interest to note that the simulations and theories overestimate the experiments in figures 1 and 3, but underestimate them in PM2 and PM4.

Turning now to the results for $NiCl_2$, we show the osmotic coefficient in figure 6 (molar scale) and in
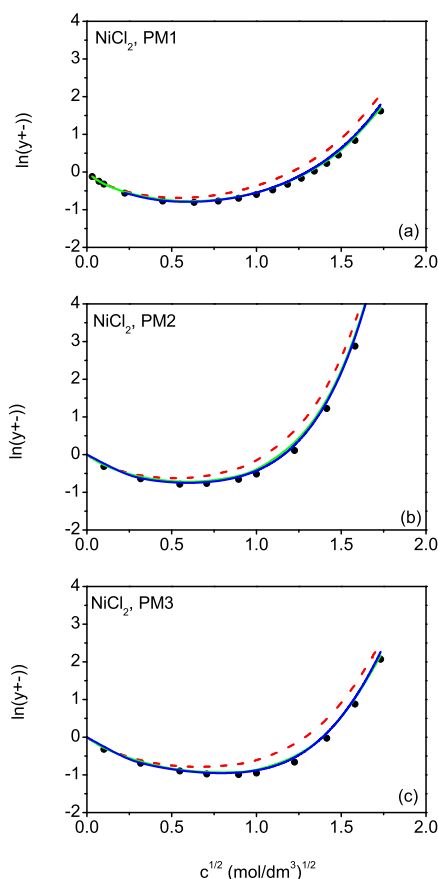
Figure 8. (Colour online) MPB, SPB, MSA, and MC mean activity coefficient $y_{\pm}$ (in molar scale) as function of square root of concentration $c^{1/2}$ (in $(mol/dm^3)^{1/2}$) for $NiCl_2$ using the PM with a concentration dependent dielectric constant ε_r. In all of the sub-figures, dashed red line SPB, solid green line MPB, solid blue line MSA, black filled circles MC. Rest of the legend as in figure 6.

figure 7 (molal scale). In figure 7 the MSA and MPB predictions match the simulations rather well for all of the three PM's, with the MSA in particular being almost quantitative with the MC data. It is noted that at higher concentrations, the agreement of these curves with the simulations is better than that seen before with $MgCl_2$. The SPB curve begins to deviate from the MC data from about $c \sim 0.25$ mol/dm^3. The behaviour of the theoretical curves and the simulation data in the molal scale in figure 7 is analogous. However, compared to the experimental results, the theoretical curves and the MC data deviate from about $m \sim 1.6$ mol/kg in PM1, $m \sim 0.6$ mol/kg in PM2, and $m \sim 1$ mol/kg in PM3, respectively.

The pattern of correspondence between the theories and the simulations continues in figures 8 and 9 where the mean activity of $NiCl_2$ is presented in molar and molal scales, respectively. In these figures, the MSA and MPB results are nearly quantitative with the MC data. The deviation shown by the SPB curve is similar to that seen for the SPB osmotic coefficient. The reason for the good agreement between the MSA, MPB and the MC, especially at higher concentrations, can be traced to the behaviour of ε_r versus c for $NiCl_2$ seen in figure1. At concentrations beyond $c \sim 1.5$ mol/dm^3, the ε_r increases leading to an overall decrease in the strength of the electrostatic interactions, which in turn lead to the observed effects. With regard to the comparative behaviour of the simulations/theories with the experimental data, the trends are analogous to that seen with the osmotic coefficient in figure 7. For PM2, there is a large deviation, but for PM1 and PM3, the deviation is relatively smaller in magnitude and also sets in at a higher concentration ($m \sim 2$ mol/kg).

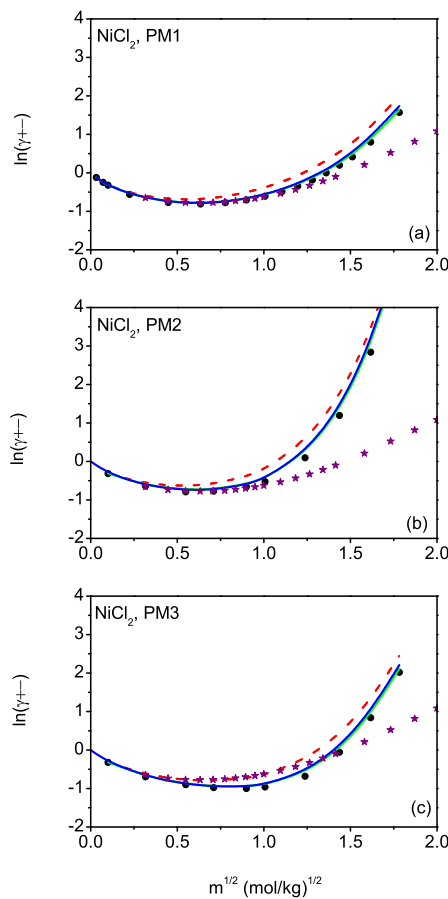**Figure 9.** (Colour online) MPB, SPB, MSA, and MC mean activity coefficient $\gamma_\pm$ (in molal scale) as function of square root of concentration $m^{1/2}$ (in $(mol/kg)^{1/2}$) for $MgCl_2$ using the PM with a concentration dependent dielectric constant ε_r. In all of the sub-figures, dashed red line SPB, solid green line MPB, solid blue line MSA, black filled circles MC, purple stars experiment [6]. Rest of the legend as in figure 6.

4. Conclusions

The work is an extension of our earlier work [28] on the thermodynamics of symmetric 1:1 valency electrolytes with variable ε_r to asymmetric 2:1 valency $MgCl_2$ and $NiCl_2$ salts. Higher and multivalencies pose a sterner theoretical challenge. As in [28], we have used experimentally determined empirical formula for ε_r as a function of concentration for both of these salts.

We have utilized the statistical mechanical formalisms of SPB, MPB, and MSA in conjunction with MC simulations, which are usually accepted as *gold standard* in this field, in order to compute the osmotic and activity coefficients of these salts. We have further compared the simulation data and the theoretical predictions with experimental results for these quantities from the literature [6].

Overall, the theoretically predicted results for ϕ_c and $y_\pm$ with the exception perhaps of that of the SPB, compare well with the corresponding simulation data. In some cases, the MSA and the MPB results are semi-quantitative or better. However, there are discrepancies at higher concentrations with the onset of such deviations occurring at lower concentrations for the SPB. For some ionic radii, combinations of $MgCl_2$, the MC data show some dispersions (beyond normal statistical error) at higher concentrations. Admittedly, in [28] the theoretical results were seen to be broadly closer to the simulations than they are in the present calculations. This is clearly due to the asymmetric 2:1 valency salts being treated here as

opposed to the symmetric 1:1 salts in [28]. With regard to the comparison with experimental data, the theories and simulations follow them reasonably well at low to intermediate concentrations. Although there are deviations at higher densities of the salts, we should emphasize that the agreement is good up to a respectable $m \sim 1$ mol/kg.

As indicated earlier, at higher concentrations, the MSA or the MPB thermodynamics reveal a relatively better agreement with the MC data for $NiCl_2$ rather than for $MgCl_2$. This occurs because the $MgCl_2$ ε_r displays a continual dielectric decrement with concentration, whereas the $NiCl_2$ ε_r actually increases at higher concentrations. For the latter, this results in dilution of the interionic interactions as the plasma coupling constant $\Gamma = e^2/(4\pi\varepsilon_0\varepsilon_r k_B T a_{+-})$ ($a_- = a_{Cl^-}$, $a_+ = a_{Mg^{2+}}$ or $a_{Ni^{2+}}$) decreases, which tends to negate somewhat the effects of higher valency.

The comparisons of simulation and theory with the experimental data show that the empirical relations (1.1) and (1.2) fail at the higher molal concentrations. A possible improvement to these empirical relations is indicated by the work of Barthel et al. [57] for non-aqueous electrolyte solutions. These authors extended their relation, equation (70), analogous to ours by using a Pade-approximant to correct for saturation effects at high concentrations.

In view of the steep increases for some of the osmotic and mean activity coefficients that occur at higher concentrations, it is tempting to wonder whether this could somehow be related to underscreening or charge inversion. At these higher concentrations, underscreening occurs, with the mean electrostatic potential displaying a damped oscillatory behavior [58]. The transformation in the mean potential is associated with the Kirkwood transition (KT) which depends on both ion size and valence. See for example [59] and the references therein. The MPB theory is based on the Kirkwood charging process and the KT identified through some critical value α_c of $\alpha = \kappa a_{ij}$. For the RPM, the present MPB does not distinguish between symmetric and unsymmetric valencies, only varying the ion size [60]. Considering solely the best fit values of PM4 for $MgCl_2$ and PM3 for $NiCl_2$, the critical values of α_c are ~0.91 and ~0.98, respectively. These values of α_c correspond to $c \sim 0.10$ mol/dm^3 and $c \sim 0.13$ mol/dm^3 for the two salts, respectively. At the highest concentration of 3 mol/dm^3, the respective values of α for $MgCl_2$ and $NiCl_2$ are 7.44 and 4.55. These values show that the rapid increase in the thermodynamic properties at the higher concentrations occurs when there is underscreening.

From a theoretical perspective, an analysis that takes into account the discreteness of the solvent rather than treating it as a continuum would be more appealing. The use of hard spheres as solvent saw a limited success since a dielectric constant needed to be assigned separately [13]. Similarly, a dipolar solvent proved less than appropriate since the predicted ε_r proved to be low for aqueous electrolytes [61]. Under the circumstances, the recourse to experimentally measured ε_r represents a more feasible way forward. Obvious advantages are the facts that the ε_r being used are more realistic and the process is more transparent.

Acknowledgements

References

1. Harned H. S., Owen B. B., The Physical Chemistry of Electrolyte Solutions, 3rd edn., Reinhold, New York, 1958.
2. Levin Y., Rep. Prog. Phys., 2002, **65**, 1577, doi:10.1088/0034-4885/65/11/201.
3. Henderson D., Holovko M., Trokhymchuk A. (Eds.), Ionic Soft Matter: Modern Trends in Theory and Applications, NATO Science Series II. Mathematics, Physics, and Chemistry Series, Vol. 206, Springer, Dordrecht, 2004.
4. Chersty A. G., Phys. Chem. Chem. Phys., 2011, **13**, 9942, doi:10.1039/c0cp02796k.
5. Robinson R. A., Stokes R. H., Electrolyte Solutions, 2nd edn., Dover, New York, 2002.
6. Barthel J., Krienke H., Kunz W., Physical Chemistry of Electrolyte Solutions: Modern Aspects, Topics in Physical Chemistry, Vol. 5, Springer, New York, 1998.

7. Outhwaite C. W., In: Statistical Mechanics, Specialist Periodical Reports, Vol. 2, Singer K. (Ed.), The Royal Society of Chemistry, 1975, 188–255, doi:10.1039/9781847556936-00188.

8. Hansen J. -P., McDonald I. R., Theory of Simple Liquids, 2nd edn., Academic Press, New York, 1990.

9. Vlachy V., Annu. Rev. Phys. Chem., 1999, **50**, 145, doi:10.1146/annurev.physchem.50.1.145.

10. McQuarrie D. A., Statistical Mechanics, University Science Books, Sausalito, 2000.

11. Friedman H. L., A Course in Statistical Mechanics, Prentice-Hall, New Jersey, 1985.

12. Blum L., Theoretical Chemistry, Advances and Perspectives, Vol. 5, Eyring H., Henderson D. (Eds.), Academic Press, New York, 1980, 1–66, doi:10.1016/b978-0-12-681905-2.50007-4.

13. Bhuiyan L. B., Vlachy V., Outhwaite C. W., Int. Rev. Phys. Chem., 2002, **21**, 1, doi:10.1080/0144235010078842.

14. Debye P., Hückel E., Z. Phys., 1923, **24**, 185.

15. Abbas Z., Ahlberg E., Nordholm S., Fluid Phase Equilib., 2007, **260**, 233, doi:10.1016/j.fluid.2007.07.026.

16. Abbas Z., Ahlberg E., Nordholm S., J. Phys. Chem. B, 2009, **113**, 5905, doi:10.1021/jp808427f.

17. Quiñones A. O., Bhuiyan L. B., Outhwaite C. W., Condens. Matter Phys., 2018, **21**, 23802, doi:10.5488/cmp.21.23802.

18. Outhwaite C. W., Bhuiyan L. B., Condens. Matter Phys., 2019, **22**, 23801, doi:10.5488/cmp.22.23801.

19. Outhwaite C. W., Bhuiyan L. B., Condens. Matter Phys., 2021, **24**, 16801, doi:10.5488/cmp.24.16801.

20. Bhuiyan L. B., Condens. Matter Phys., 2021, **24**, 23801, doi:10.5488/cmp.24.23801.

21. Hückel E., Z. Phys., 1925, **26**, 93.

22. Shilov I. Y., Lyashchenko A. K., J. Phys. Chem. B, 2015, **119**, 10087, doi:10.1021/acs.jpcb.5b04555.

23. Triolo R., Blum L., Floriano M. A., J. Chem. Phys., 1978, **67**, 5956, doi:10.1063/1.434805.

24. Simonin J.-P., Blum L., Turq P., J. Phys. Chem., 1996, **100**, 7704, doi:10.1021/jp953567o.

25. Fawcett W. R., Tikanen A. C., J. Phys. Chem., 1996, **100**, 4251, doi:10.1021/jp952379v.

26. Tikanen A. C., Fawcett W. R., J. Electroanal. Chem., 1997, **439**, 107, doi:10.1016/s0022-0728(97)00376-8.

27. Abbas Z., Ahlberg E., J. Solution Chem., 2019, **48**, 1222, doi:10.1007/s10953-019-00905-y.

28. Quiñones A. O., Bhuiyan L. B., Abbas Z., Outhwaite C. W., J. Mol. Liq., 2023, **371**, 12119, doi:10.1016/j.molliq.2022.121119.

29. Friedman H. L., J. Chem. Phys., 1982, **76**, 1092, doi:10.1063/1.443076.

30. Levy A., Andelman D., Orland H., Phys. Rev. Lett., 2012, **108**, 227801, doi:10.1103/physrevlett.108.227801.

31. Valiskó M., Boda D., J. Chem. Phys., 2014, **140**, 234508, doi:10.1063/1.4883742.

32. Gavish N., Promislow K., Phys. Rev. E, 2016, **94**, 012611, doi:10.1103/physreve.94.012611.

33. Adar R. M., Markovich T., Levy A., Orland H., Andelman D., J. Chem. Phys., 2018, **149**, 054504, doi:10.1063/1.5042235.

34. Hasted J. B., Ritson D. M., Collie C. H., J. Chem. Phys., 1948, **16**, 1, doi:10.1088/0959-5309/60/2/304.

35. Lobo H. M. M., Quaresma J. L., Handbook of Electrolyte Solutions, Part B, Elsevier, Amsterdam, 1989.

36. Stokes R. H., Trans. Faraday Soc., 1945, **41**, 642, doi:10.1039/tf9454100642.

37. Stokes R. H., Trans. Faraday Soc., 1948, **44**, 295, doi:10.1039/tf9484400295.

38. Stokes R. H., Robinson R. A., J. Am. Chem. Soc., 1948, **70**, 1870, doi:10.1021/ja01185a065.

39. Svensson Bo R., Woodward C. R., Mol. Phys., 1988, **64**, 247, doi:10.1080/00268978800100203.

40. Rasaiah J. C., Friedman H. L., J. Chem. Phys., 1968, **48**, 2742, doi:10.1063/1.1669510.

41. Outhwaite C. W., Molero M., Bhuiyan L. B., J. Chem. Soc., Faraday Trans., 1991, **87**, 3227, doi:10.1039/FT9918703227.

42. Outhwaite C. W., Molero M., Bhuiyan L. B., J. Chem. Soc., Faraday Trans., 1993, **89**, 1315, doi:10.1039/FT9938901315.

43. Outhwaite C. W., Molero M., Bhuiyan L. B., J. Chem. Soc., Faraday Trans., 1994, **90**, 2002, doi:10.1039/FT9949002001.

44. Ulloa-Dávilla E. O., Bhuiyan L. B., Condens. Matter Phys., 2017, **20**, 43801, doi:10.5488/cmp.20.43801.

45. Leonard P. J., Henderson D., Barker J. A., Mol. Phys., 1971, **21**, 107, doi:10.1080/00268977100101221.

46. Grundke E. W., Henderson D., Mol. Phys., 1974, **24**, 269, doi:10.1080/00268977200101431.

47. Verlet L., Weis J. J., Phys. Rev. A, 1972, **5**, 939, doi:10.1103/physreva.5.939.

48. Molero M., Outhwaite C. W., Bhuiyan L. B., J. Chem. Soc., Faraday Trans., 1992, **88**, 1541, doi:10.1039/FT9928801541.

49. Ebeling W., Scherwinski K., Z. Phys. Chem. (Leipzig), 1983, **264**, 1, doi:10.1515/zpch-1983-26402.

50. Outhwaite C. W., Bhuiyan L. B., Vlachy V., Hribar-Lee B., J. Chem. Eng. Data, 2010, **55**, 4248, doi:10.1021/je100394d.

51. Blum L., Mol. Phys., 1975, **30**, 1529, doi:10.1080/00268977500103051.

52. Blum L., Hoye J. S., J. Phys. Chem., 1977, **30**, 1529, doi:10.1021/j100528a019.

53. Sanchez-Castro C., Blum L., J. Phys. Chem., 1989, **93**, 7478, doi:10.1021/j100358a043.

54. Bellman R., Kalaba R., Quasilinearization and Nonlinear Boundary Value Problems, Elsevier, New York, 1965.

55. Martinez M. M., Bhuiyan L. B., Outhwaite C. W., J. Chem. Soc., Faraday Trans., 1990, **86**, 3383, doi:10.1039/FT9908603383.
56. Buchner R., Hefter G., Phys. Chem. Chem. Phys., 2009, **11**, 8984, doi:10.1039/b906555p.
57. Barthel J., Krienke H., Holovko M. F., Kapko V. I., Protsykevich I. A., Condens. Matter Phys., 2000, **23**, 657, doi:10.5488/cmp.3.3.657.
58. Outhwaite C. W., Bhuiyan L. B., J. Chem. Phys., 2021, **155**, 014504, doi:10.10635/5.0054203.
59. Dinpajooh M., Biasin E., Nienhuis E. T., Mergelsberg S. T., Benmore C. J., Schenter G. K., Fulton J. L., Kathmann S. M., Mundy C. J., J. Chem. Phys., 2024, **161**, 151102, doi:10.1063/5.0234518.
60. Thomlinson M. M., Outhwaite C. W., Mol. Phys., 1982, **47**, 1113, doi:10.1080/00268978300100812.
61. Kournopoulos S., Haslam A. J., Jackson G., Galindo A., Schöen M., J. Chem. Phys., 2022, **156**, 154111, doi:10.1063/5.0079511.

Вплив змінної відносної діелектричної проникності на термодинаміку асиметричної валентності водних солей

А. О. Квінонес[1], З. Аббас[2], К. В. Оусвейт[3], Л. Б. Буіян[1]

[1] Лабораторія теоретичної фізики, Фізичний факультет університету Пуерто-Ріко, 17 Авеніда Університад, STE 1701, Сан Хуан, Пуерто-Ріко 00925-2537, США

[2] Факультет хімії та молекулярної біології університету Ґетеборга, Кенінгарден 4, SE-41296, Ґетеборг, Швеція

[3] Вища школа математики та фізики, університет Шеффілда, Шеффілд S3 7RH, Великобританія

Експериментально визначені емпіричні формули для залежної від концентрації відносної діелектричної проникності водних розчинів $MgCl_2$ і $NiCl_2$ використовуються для розрахунку осмотичного коефіцієнта та середнього коефіцієнта активності цих солей у широкому діапазоні концентрацій. Системи моделюються за допомогою примітивної моделі електролітів та аналізуються на основі симетричної теорії Пуассона-Больцмана, модифікованої теорії Пуассона-Больцмана, середньо-сферичного наближення та моделювання Монте-Карло. Загалом, середньо-сферичне наближення та модифікована теорія Пуассона-Больцмана добре відтворюють дані *еталонного* моделювання до концентрацій ~1,6 моль/дм^3 і більше, тоді як симетричні результати Пуассона-Больцмана мають певні відхилення, починаючи з ~0,25 моль/дм^3. Як правило, і моделювання, і теорії, приводять до похибок у порівнянні з відповідними експериментальними результатами при концентраціях понад ~1 моль/кг.

Ключові слова: *примітивні моделі електролітів, осмотичний коефіцієнт та коефіцієнт активності, моделювання Монте-Карло, симетризовані та модифіковані теорії Пуассона-Больцмана*